SUPPORTING INFORMATION

Dynamics, hydration, and motional averaging of a loop-gated artificial protein cavity: the W191G mutant of cytochrome *c* peroxidase in water as revealed by molecular dynamics simulations

Riccardo Baron and J Andrew McCammon

Supplementary tables

Table S1. Solute-solvent hydrogen-bond occurrences to labeled water molecules in proximity of the W191G cavity[a]

system	H-bond donor – acceptor	occurrence %		system	H-bond donor – acceptor	occurrence %	
		simulation	X-ray Structure			simulation	X-ray structure
ref	NH(Phe 202) – wt 309[b]	58.9	100	open	NEH(Arg 48) – wt 300[b]	5.5	100
	CE2H(Phe 202) – wt 309[b]	19.5			NH2(Arg 48) – wt 300[b]	36.4	
	OH(Thr 234) – wt 332	79.9	100		NH(Asn 195) – wt 452	24.3	100
bb	NH1(Arg 48) – wt 300	9.9	100		wt 302 – O(heme O2D)[b]	26.4	100
	NH(Gly 191) – wt 308	92.5	100		wt 302 – O(heme O1A)[b]	7.9	

a. The hydrogen-bond donors and acceptors are specified in the second column (with residue name and sequence numbers defined based on the GROMOS96 force field (*53*)). Water molecules (wt) forming hydrogen bonds are labeled with reference to the corresponding PDB data (*57*). Relative values of occurrences from simulation and corresponding X-ray structures are given in the third and fourth columns, respectively. Only hydrogen bonds occurring for at least 5% of the time are reported. See Table 1 for reference codes and Methods section for computational details.

b. Part of a multi-center hydrogen bond.

Supplementary figures

Figure S1 Time series of the secondary structure of the W191G cavity mutant of cytochrome *c* peroxidase for (a) **ref**, (b) **bb**, and (c) **open** simulations. Top-right panels: backbone C^{α} atom-positional root-mean-square fluctuations (RMSF) along the amino acid sequence. Bottom-left panels: backbone atom-positional root-mean-square deviation (RMSD) of trajectory structures from the experimental X-ray structure as a function of time. See Table 1 for reference codes and Methods section for computational details.

Figure S2 Stability of the heme cofactor during the MD simulations. (a) Timeseries of the distance between Asp 235 and the Fe atom in the heme co-factor. (b) Root-mean-square fluctuation (RMSF) along the heme cofactor atom sequence. The most pronounced peaks correspond to the O1A and O2A carboxy-acid oxygens, the CBB and CBC carboxyl oxygens, and the O1D and O2D carboxy-acid oxygens (atom sequence nr. 17, 18, 26, 35, 46, and 47, respectively). The nomenclature of atom groups is defined based on the GROMOS96 force field (*53*). Color coding refers to **ref** (black), **bb** (red), **open** (green), **rst** (blue), and **rsto** (cyan) simulations. See Table 1 for reference codes.

Figure S3 Normalized-probability distributions of the Asn 295 – ion distances. Color codes refer to **ref** (black), **bb** (red), **open** (green), **rst** (blue), and **rsto** (cyan) simulations. The distances were calculated between the aliphatic carbon of the Asn 295 side chain and all K^+ ions in each system (see Table 1). The presence of ions into the cavity of W191G can be clearly noticed for **ref**, and in smaller extent for **rst** and **rsto** simulations.

Figure S4 Backbone torsional-angle normalized-probability distributions characterizing the loop-gating mechanism around the two hinge points of residues Pro 190 and Asn 195. The *cis-trans* isomerization is described by a shift of average value for the torsional angle ω of Pro 190 (C^{α} – C – N – $C^{\alpha,\,ring}$) between closed (300 K: **ref**, **bb**; 500 K with constraining potential: **rst**) and open (300 K: **open**; 500 K with constraining potential: **rsto**) state ensembles (top panels). Corresponding rotations around the ϕ and ψ angles of Asn 195 can be quantified comparing the same simulation ensembles (middle and bottom panels, respectively). The vertical dashed lines indicate the dihedral-angle values based on the reference X-ray structures (*57*). See Table 1 for reference codes.

Figure S5 Time series of (a) the solvent-accessible surface area (SASA) for *all* atom trajectory structures and (b) the radius of gyration (RGYR) of the W191G cavity atoms. Graphs refer to **ref** (black thick lines), **bb** (black thin lines), **open** (grey thick lines), **rst** (dotted black lines), and **rsto** (dotted grey lines) simulations, respectively. For graphical purposes running averages (over periods of 10 ps) are shown. See Table 1 for reference codes and Methods section for computational details.

Figure S6 Radial distribution functions $g(r)$ and their integrals for the water oxygens of **ref**, **bb**, **open**, **rst**, and **rsto** simulations. The functions were centered on the side-chain aliphatic carbon of Asp 235 and calculated based on the entire 10 ns (black lines) or on the last 2 ns simulation periods (grey lines). The corresponding running integrals ξ of $4\pi r^2 \rho\, g(r)$ are also shown (dashed black and gray lines, respectively). See Table 1 for reference codes.

FIGURE S1

a)

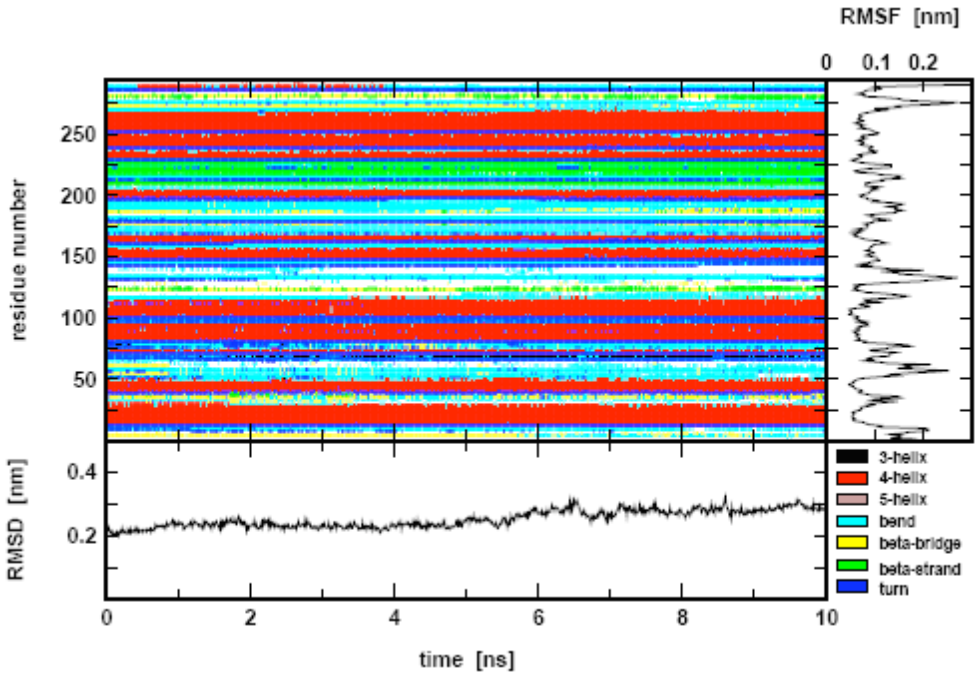
RMSF [nm]
0 0.1 0.2
residue number
250
200
150
100
50
RMSD [nm]
0.4
0.2
0 2 4 6 8 10
time [ns]
3-helix
4-helix
5-helix
bend
beta-bridge
beta-strand
turn

b)

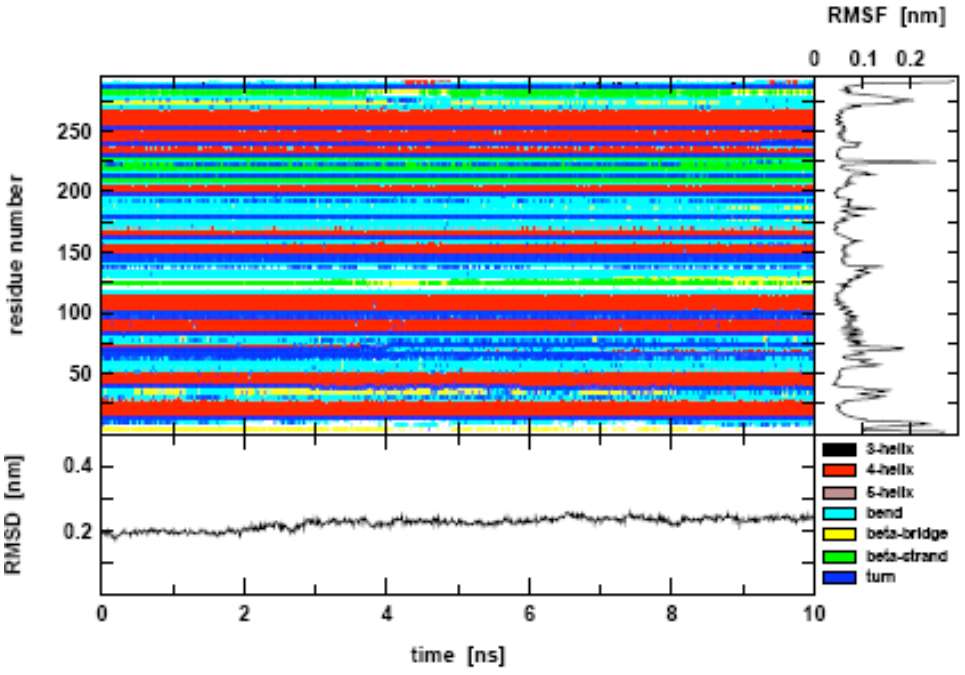
RMSF [nm]
0 0.1 0.2
residue number
250
200
150
100
50
RMSD [nm]
0.4
0.2
0 2 4 6 8 10
time [ns]
3-helix
4-helix
5-helix
bend
beta-bridge
beta-strand
turn

c)

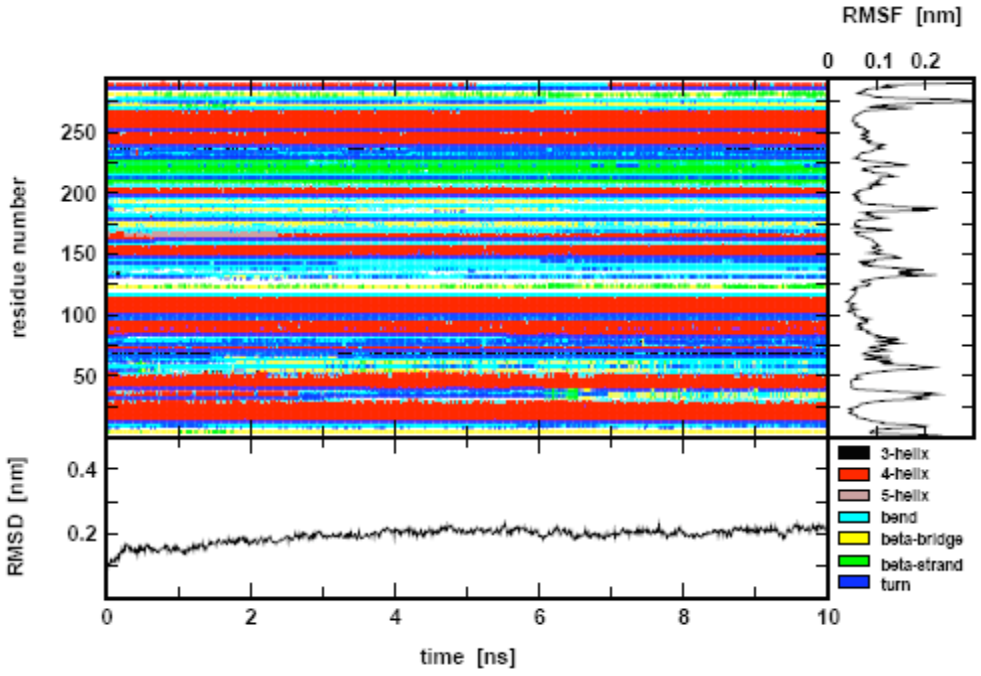
RMSF [nm]
0
0.1
0.2
residue number
250
200
150
100
50
RMSD [nm]
0.4
0.2
0
2
4
6
8
10
time [ns]
3-helix
4-helix
5-helix
bend
beta-bridge
beta-strand
turn

FIGURE S2

a)

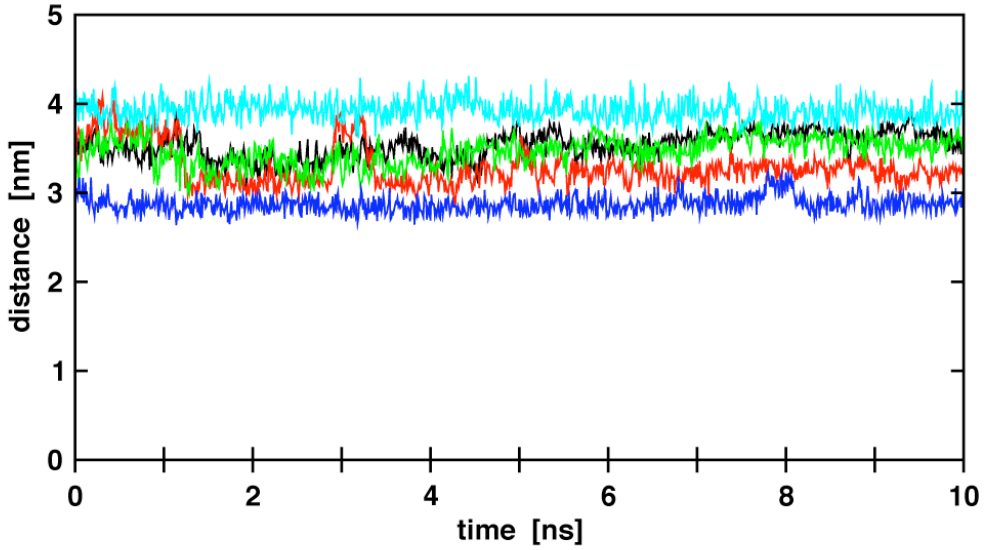
distance [nm]
time [ns]
0
1
2
3
4
5
0
2
4
6
8
10

b)

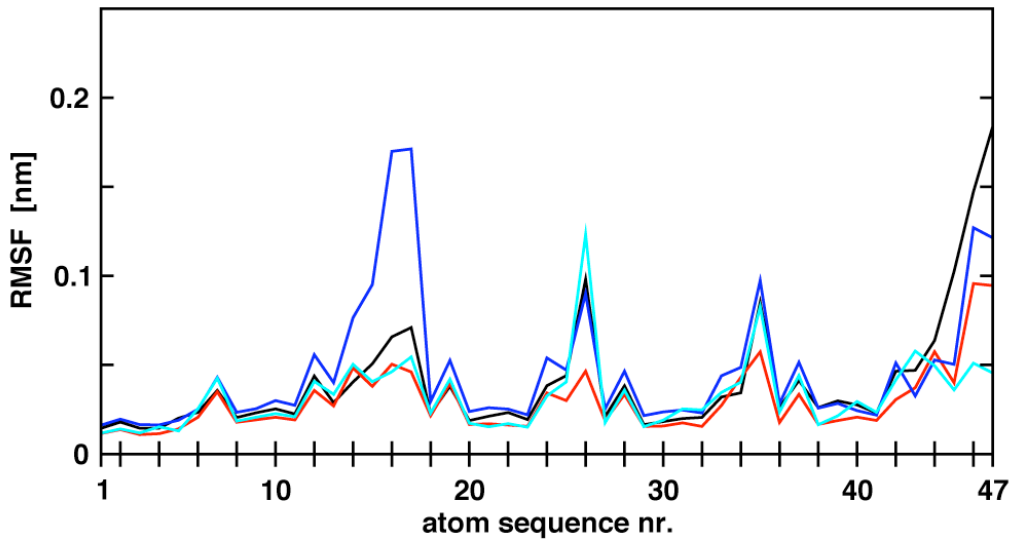
RMSF [nm]
atom sequence nr.
0
0.1
0.2
1
10
20
30
40
47

FIGURE S3

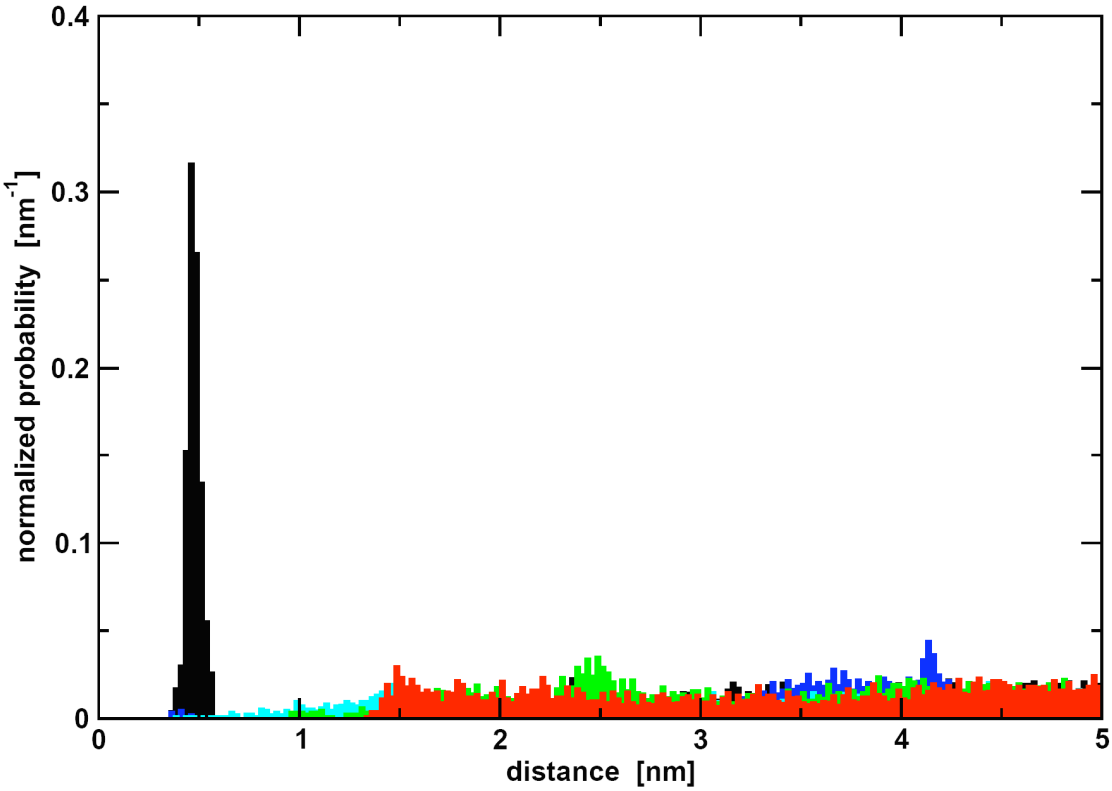

FIGURE S4

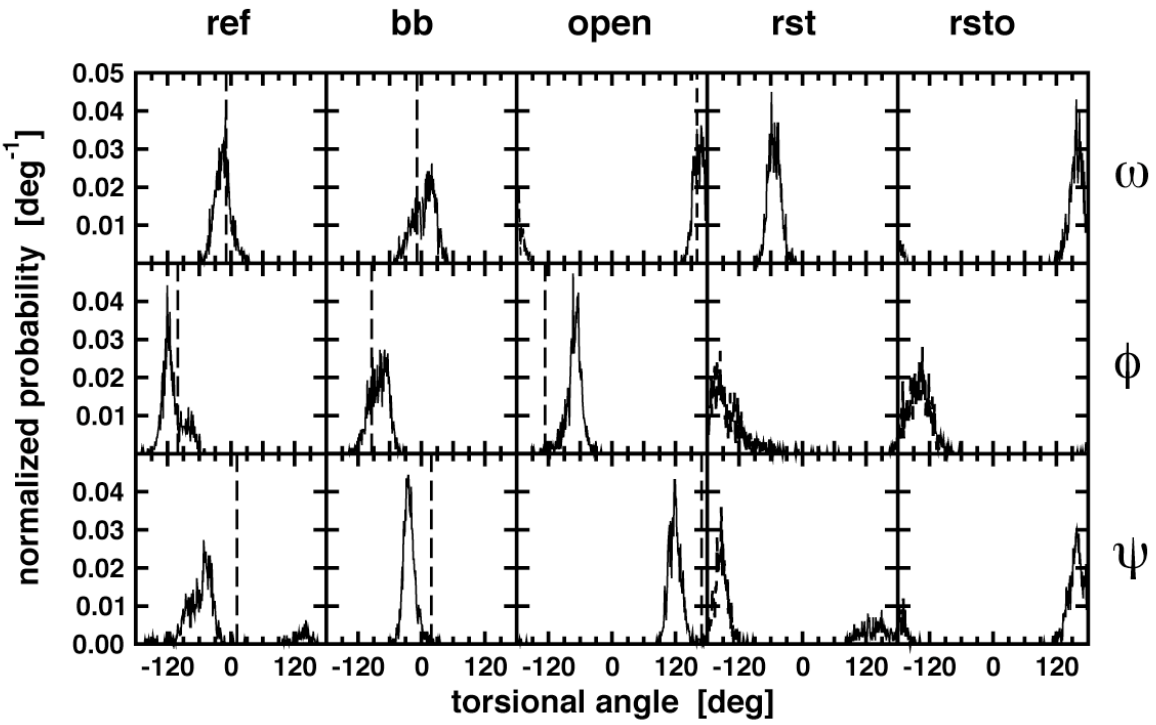
ref
bb
open
rst
rsto
normalized probability [deg^{-1}]
0.05
0.04
0.03
0.02
0.01
0.00
ω
ϕ
ψ
-120
0
120
torsional angle [deg]

FIGURE S5

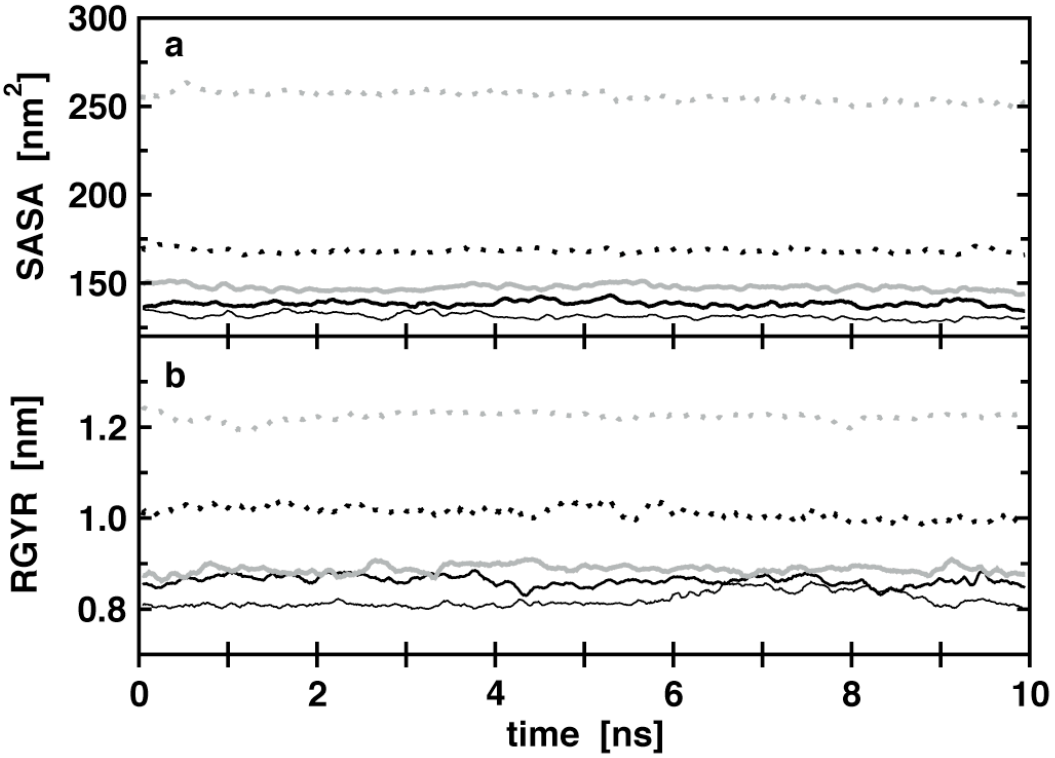

FIGURE S6